AIChE

A Numerical Study of Mixing in a Microchannel with Circular Mixing Chambers

Mubashshir Ahmad Ansari and Kwang-Yong Kim
Dept. of Mechanical Engineering, Inha University, Incheon 402-751, Republic of Korea

DOI 10.1002/aic.11833
Published online July 6, 2009 in Wiley InterScience (www.interscience.wiley.com).

The mixing of fluids in a microchannel is numerically investigated using three-dimensional Navier–Stokes equations. The microchannel has circular mixing chambers that are designed to create a self-circulating flow that operates at low Reynolds numbers. The investigations have been performed on a design that comprises of four circular mixing chambers that are joined together with constriction channels. The study has been carried out in two parts. Firstly, the mixing and the flow field are analyzed for a wide range (1–250) of the Reynolds number. Secondly, the effects of two design parameters, namely, the ratio, w/d, of the width of the constriction channel to the diameter of the circular chamber, and the angle, θ, between the outer walls of the chamber and the connection channel, on the mixing and the flow field have been evaluated. The mixing has been evaluated using a parameter, called mixing index, which is based on the variance of the mass fraction. The mixing index at the end of the device increases rapidly with the Reynolds number. The presence of a flow recirculation zone in the circular chamber is found to be effective in enhancing mixing, especially for larger Reynolds numbers. The mixing performance improves with an increase in θ, and with a decrease in w/d. The characteristics of the pressure drop have also been investigated as a function of the Reynolds number and geometric parameters.
 AIChE J, 55: 2217–2225, 2009
Keywords: mixing, microchannel, circular chamber, numerical analysis, diffusion

Introduction

Microfluidic devices are required for many applications in chemical and biological analysis. The flow in these devices is predominantly laminar, which limits the rate at which solutions mix. Enhancement of the mixing rate is a critical issue for several microfluidic applications. Researchers have investigated mixing on a microscale and have developed new micromixers, many of which operate under different principles (Nguyen et al.[1] and Hessel et al.[2]). Broadly, micromixers can be classified as active and passive micromixers. An active micromixer uses external energy, such as electric or magnetic energy, to manipulate the flow field to control the mixing process.

Passive micromixers require no such external energy, and are easy to fabricate and operate, when compared with active micromixers. Numerous passive micromixers, operating under various principles, have been reported in the literature. Micromixers with a curved channel or circular mixing chambers are found to be effective in mixing. Dean vortices are formed when the fluid flow experiences centrifugal force in a curved channel. With regard to fluid flow in helical, coiled, circular tubes, Dean[3,4] found a pair of symmetrical vortices in the cross-sectional plane, arising from centrifugal force. The magnitude of these vortices is characterized by a dimensionless Dean number ($De = Re/\sqrt{\lambda}$), where λ is the ratio of the hydrodynamic radius of the channel to the radius of curvature of the channel. Numerous studies on the effect of

Correspondence concerning this article should be addressed to K.-Y. Kim at kykim@inha.ac.kr

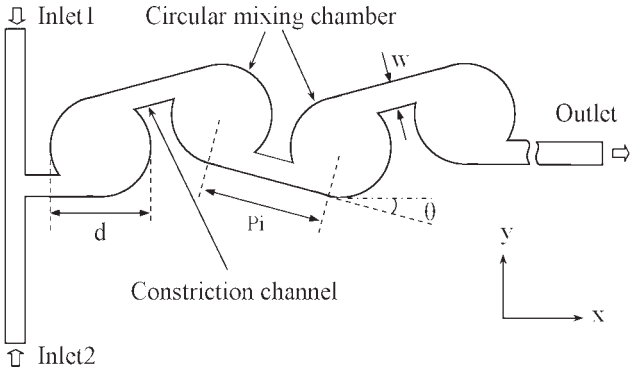

Figure 1. Schematic of the micromixer with circular chambers.

Dean flows in the mixing of fluids can be found in the literature.[5–10] Sudarshan and Uzag[7] analyzed mixing in a compact, spiral-shaped microchannel at Reynolds numbers ranging from 0.02 to 18.6. At higher Reynolds numbers, secondary Dean effects are developed that increase mixing, while at lower Reynolds numbers mixing is governed mainly by diffusion. Sudarshan and Uzag[8] also analyzed mixing in planar, two-dimensional microchannels by introducing curvature and varying channel widths.

Vanka et al.[9] performed numerical analysis on the rates of mixing in a curved square duct at low Reynolds numbers. Kumar et al.[10] reported an analysis of mixing in a curved microchannel with a circular cross-section for various Reynolds numbers, Schmidt numbers, and curvature ratios. For fluids with higher Schmidt numbers, mixing is considerably improved at $Re \sim 10$ but is unaffected at $Re \sim 0.1$, which is also the case in the results of Vanka et al.[9] Yamaguchi et al.[11] reported an analysis of mixing in microchannels with hairpin curves.

Hong et al.[12] reported an analysis of mixing in Tesla structures over a wide range of flow rates; the structures were found to be effective for mixing at higher flow rates. The mixing performance is influenced by both diffusion and convection. Lee and Lee[13] investigated the effect of rotation in split and recombination (SAR) mixing in a microchannel. They designed three types of SAR micromixers that were defined by the rotation effect and by the direction of rotation. Chang and Cho[14] designed and fabricated micromixers that are comprised of 3D rotationally arranged microblocks and dividing microchannels that induce swirl flow. The design is found to be capable of creating repeated rotational flow fields that can mix fluid for a wide range of flow rates.

Park et al.[15] designed a passive micromixer that induces fluid rotation to mix fluids at both low and high Reynolds numbers. The rotation of fluid increases the interfacing of the two fluids through stretching and folding. Jeon et al.[16] proposed a passive micromixer with side channels to create recycle flows at Re 7, 14, and 28. Computational fluid dynamics was applied to design and optimize the geometry for creating recycle flow. Mixing is enhanced by the flow circulation that is developed in the main body of the micromixer.

Lin et al.[17,18] proposed a three-dimensional micromixer comprising of a circular mixing chamber and based on the idea of inducing self rotation. They carried out experimental and numerical analysis to study the flow and mixing behavior of the device. The three-dimensional vortices are generated in the circular chamber by injecting fluid from inlets that are tangentially aligned at one end of the chamber.

Chung et al.[19] reported a passive micromixer with in-plane circular chambers that induce self-circulation to the flow. The inlet and outlet channels to the circular mixing chamber were designed at a tangent to the chamber to create recirculation flow in the chamber, which causes fluid to mix. The formation of self-circulation is depicted at a critical Reynolds number ($Re = 20$) near the inlet to the chamber.

Jin et al.[20] also reported the mixing performance, as a function of Reynolds numbers and the mass fraction of glycerol in water, of a micromixer with a circular mixing chamber that creates swirl flow. The formation of swirl flow is depicted at higher Reynolds numbers and accelerates mixing. Hu and Chang[21] investigated mixing and the characteristics of the pressure drop for a circular chamber and various fluids.

It is obvious from the above literature on circular mixing chambers that the circulation flow in the chambers enhances mixing. The ratio of the diameter of the circular chamber to the width of the inlet channel is likely to be the most important parameter that influences the flow field and mixing performance of the devices. However, previous studies have fixed the value of this parameter, instead of varying it. The integration of the present, circular chamber into a series of chambers, which are connected with each other through constriction channels that are tangentially oriented, is likely to be more effective for mixing in lieu of a back-and-forth motion for enhancing mixing in a single chamber.

In the present investigation, numerical analyses of the mixing of two fluids have been performed in a geometry that comprises of four circular mixing chambers that are connected in series by constriction channels, as shown in Figure 1. The constriction channels that join the circular mixing chambers are tangentially aligned for creating flow circulation. The study has been carried out in two stages. Firstly, mixing and flow field analysis have been performed at Reynolds numbers ranging from 1 to 200 for a fixed ratio, w/d, of the width of the constriction channel to the diameter of the circular chamber. Secondly, the effects of two geometric parameters, i.e., w/d and the angle, θ, between the outer walls of the chamber and the connection channel (Figure 1), on mixing performance and the characteristics of the pressure drop have been analyzed for a fixed Reynolds number.

Physical Model and Numerical Analysis

Figure 1 shows a schematic model of the microchannel with four circular mixing chambers, each with a diameter of 800 μm, which are connected with constriction channels to create self-circulating flow. The cross-section of the microchannel is rectangular. The distance, P_i, between the centers of two consecutive chambers is fixed at 1×10^{-3} m. The width, w, of constriction channels that join the circular chambers is varied for examining its influence on the mixing and the flow field. The second design parameter, θ, is varied with the aim of providing more turn to the motion of fluid in the circular chamber. The parameters, w/d and θ, are varied from 1/8 to 1/4 and from 0° to 25°, respectively. The height

of the model has been kept constant at 100 μm for all calculations. The inlet to the channel is so aligned as to smoothly introduce fluid into the mixing chamber for creating self-circulating flow.

The two inlets, Inlet 1 and Inlet 2, are merged into the main microchannel with a T-joint, as shown in Figure 1. Water and ethanol are selected as two working fluids for mixing. The properties of water and ethanol are taken for a temperature of 20°C; the densities of water and ethanol accordingly are 998 and 789 kg m^{-3}, respectively. The Reynolds number is calculated based on the dimension of the constriction channel and the property of water.

A computational analysis of fluid dynamics has been performed using the commercial code, ANSYS CFX-11.0,[22] which is a general-purpose code that solves Navier–Stokes equations using the finite-volume-method via a coupled solver. ANSYS CFX is capable of modeling fluid mixtures comprised of many separate physical components where each component may have a distinct set of physical properties. In case of multicomponent fluids, assumptions are made that the fluids are mixed at molecular level, and they have the same mean velocity, pressure, etc. Hence, the bulk motion of the fluid is modeled using single velocity, pressure, etc., while each component has its own equation for the conservation of mass which can be expressed as;

$$\frac{\partial(\rho_i V_j)}{\partial x_j} = -\frac{\partial}{\partial x_j}(\rho_i(V_{ij} - V_j)) \tag{1}$$

$$V_j = \sum(\rho_i V_{ij})/\overline{\rho} \tag{2}$$

$$\rho_i(V_{ij} - V_j) = -\frac{\Gamma_i}{\overline{\rho}}\frac{\partial \rho_i}{\partial x_j} \tag{3}$$

where ρ_i is the density of the fluid component i in the mixture, i.e., the mass of the fluid component i per unit volume. V_j is the average velocity field, $\rho_i (V_{ij} - V_j)$ is the relative mass flux and V_{ij} is the velocity of fluid component i. The differential motion of the individual components in the mixture is accounted by the relative mass flux term. This term may be modeled in a number of ways to include the effects of concentration gradients, pressure gradients, etc. The concentration gradient is the primary effect of the possible relative motion of the mixture components.

$$\Gamma_i = \rho D_i$$

Γ_i and D_i are the molecular diffusion coefficient and diffusivity of fluid component i, respectively. When all the Eqs. 1 are summed over all fluid components, the result is standard continuity equation expressed as;

$$\frac{\partial(\overline{\rho} V_j)}{\partial x_j} = 0 \tag{4}$$

The momentum (Navier–Stokes) equations solved in this work are represented as follows.

$$\overline{\rho}(\vec{V} \cdot \nabla)\vec{V} = \nabla p + \mu \nabla^2 \vec{V} \tag{5}$$

For each of multiple component fluids, a single velocity is calculated in the simulation. Each individual component of fluids flows with the velocity of the multi component, with drift velocity superimposed which arises from diffusion. For each control volume in the flow domain, the appropriate average value of the properties is evaluated for use in calculating the flow field. It is assumed that the mass transfer takes place by convection and diffusion. A further assumption is that the diffusion velocity of a component fluid obeys Fick's Law. This average value depends on the property of the component fluids and the proportion of the fluids in the control volume. One component of the fluid is assigned constraint equation which ensures to evaluate its mass fraction by subtracting the sum of the mass fraction of the other fluid components from unity. The addition of mass fraction of the components must be equal to 1.

ANSYS ICEM 11.0 was used to make hexahedral grids for the full model. A high-quality grid system is critical for achieving accurate results, especially for analyses of mixing, due to the presence of numerical diffusion. In the present case, the advection terms have been discretized by using a bounded second-order differencing scheme, which is an upwind scheme with a second-order correction.[22] While numerical diffusion cannot be completely ignored, it can be minimized by adopting certain techniques,[23,24] such as second-order discretization techniques and the adjustment of grid cells for aligning their edges with the direction of the local flow velocity. Numerical diffusion is present even for very fine computational grids with large numbers of nodes. The grids cells of the full model should be checked as any misalignment in a few cells introduces numerical diffusion.[25] Normal velocity at the two inlets and zero static pressure at the outlet have been applied as the boundary conditions. One half of the full domain is set as the computational domain, and the condition of symmetry has been applied on the symmetric plane. No slip boundary conditions have been assigned for the solid walls. The solutions are considered to have attained convergence for an rms value of 10^{-6}.

The quantification of mixing is accomplished by calculating the variance of the species in the micromixer. The variance is based on the concept of the intensity of segregation, which, in turn, is based upon the variance of the concentration with the mean concentration. To evaluate the degree of mixing in the micromixer, the variance of the mass fraction of the mixture in a cross-section that is normal to the direction of flow is defined as:

$$\sigma = \sqrt{\frac{1}{N}\sum(c_i - \overline{c}_m)^2} \tag{6}$$

where N is the number of sampling points inside the cross-section, c_i is the mass fraction at sampling point i, and $\overline{c}_m$ is the optimal mixing mass fraction. In this work, on each plane, N exceeds 400 for ensuring high accuracy, and the sampling points are equidistant on the cross-sectional plane. The values at the sampling points are obtained by interpolations with the values at adjacent computational grids. As given below, the mixing index at various locations along the direction of flow is so defined as to evaluate the degree of mixing of the fluids in a plane that is perpendicular to the direction of flow.

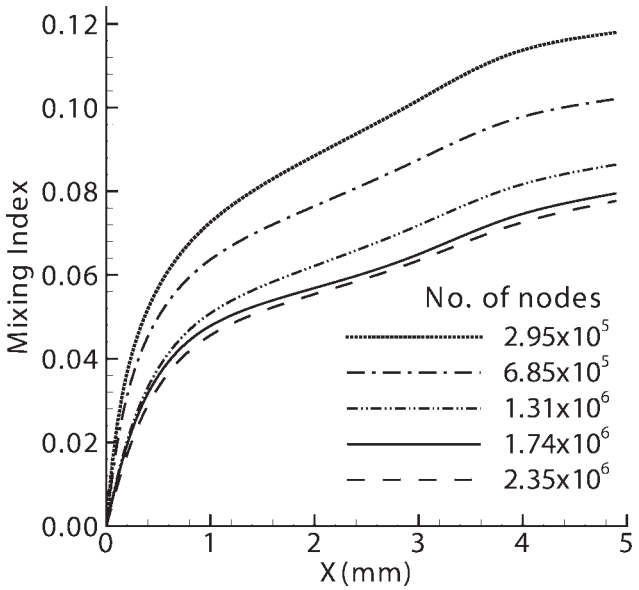

Figure 2. Test of grid independency ($\theta = 0^\circ$ and $d/w = 1/8$).

$$M = 1 - \sqrt{\frac{\sigma^2}{\sigma^2_{\max}}} \tag{7}$$

In Eq. 7, $\sigma_{\max}$ is the maximum variance over the range of data. The variance is maximal for completely unmixed fluids and minimal for completely mixed fluids. For comparing the results, the mixing index has been calculated on a plane after every circular mixing chamber.

Results and Discussion

Figure 2 shows results of the preliminary test of grid independency with five different grid systems wherein the number of nodes varies from 2.92×10^5 to 2.35×10^6. The distribution of the mixing index along the x-axis on the planes between the circular mixing chambers has been evaluated for the test of grid independency. The test has been performed for the geometry corresponding to $\theta = 0^\circ$ and $d/w = 1/8$. For coarser grids, the distributions of the mixing index show significant variation as the number of nodes increases. At the exit of the last circular mixing chamber, the relative change in the mixing index between the grid systems corresponding to 1.74×10^6 and 2.35×10^6 nodes, respectively, is only 2.21%. Finally, among the tested grid systems, the grid system with 1.74×10^6 nodes has been selected for further analyses.

Figure 3 shows a comparison of the present computational results with the experimental results of Chung et al.,[19] for the same w/d ratio and Reynolds number. The vectors have been plotted on a xy-plane at the middle of the channel. The computational results show the presence of a single circulation zone near the inlet to the circular chamber as do the experimental results[19] The computational flow field in a circular mixing chamber at $Re = 50$ is, qualitatively speaking, in good agreement with the experimental results, as seen from Figure 3.

Mixing and flow field analysis

The mixing and flow field analysis have been carried out for a fixed geometry with $\theta = 0^\circ$ and $w/d = 1/8$. Figure 4 shows the plot for the mixing index at the exit of the fourth (and last) circular mixing chamber for Reynolds numbers, Re, equaling 1, 5, 10, 25, 50, and 150, and for $\theta = 0^\circ$ and $w/d = 1/8$. The mixing index is minimum at $Re = 5$. Mixing at a lower Reynolds number, $Re = 1$, is likely due to the diffusion of fluid molecules, as a result of the longer time of residence of the fluids in the chambers. However, for Reynolds numbers exceeding five, the trend shows an increase in the mixing index with the Reynolds number—even though the time of residence decreases. This is likely due to an increase in the inertial force—with an increase in the Reynolds number—that promotes the structure of re-circulating flow in the circular chamber and thus, the mixing of the fluids.

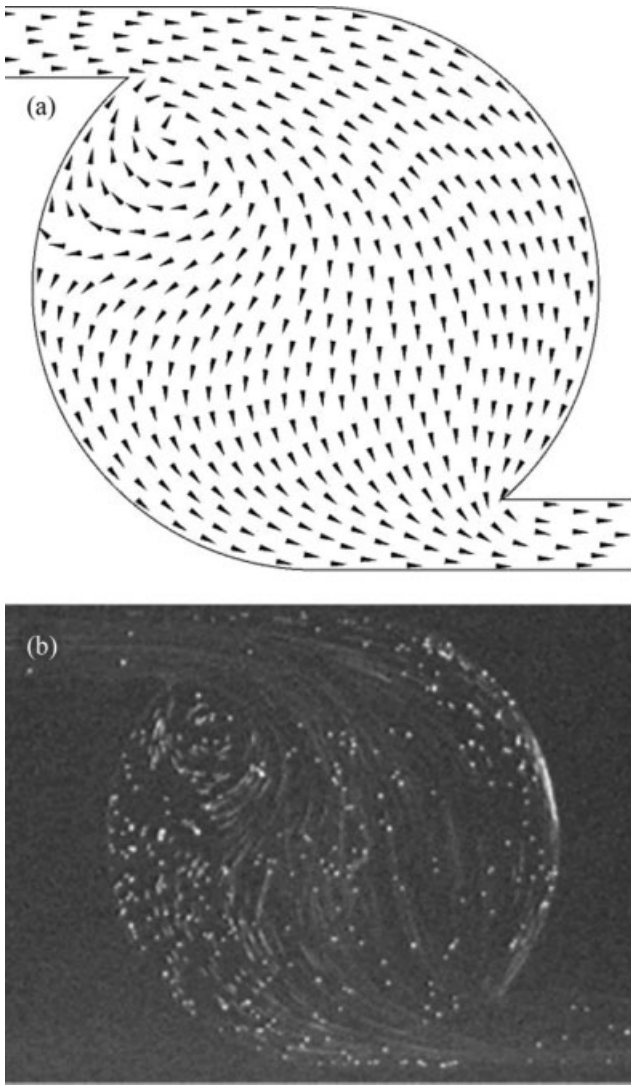

Figure 3. Comparison with experimental results at $Re = 50$.

(a) Vector plot for present numerical simulation and (b) experimental results.[19]

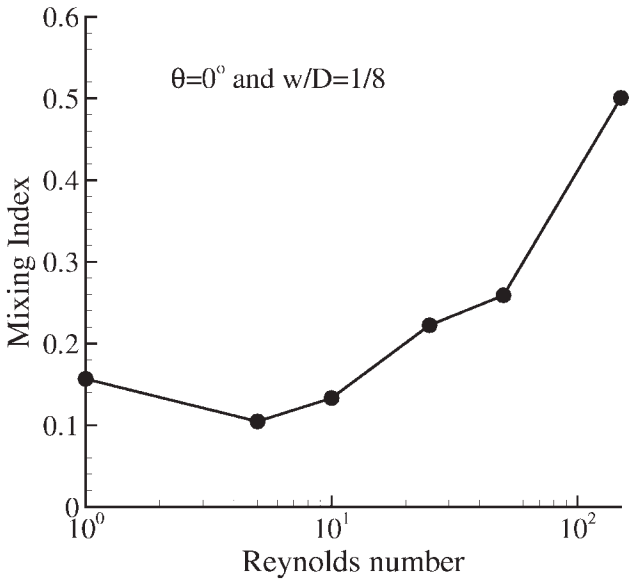

Figure 4. Variation of the mixing index with the Reynolds number, at the exit of the last mixing chamber.

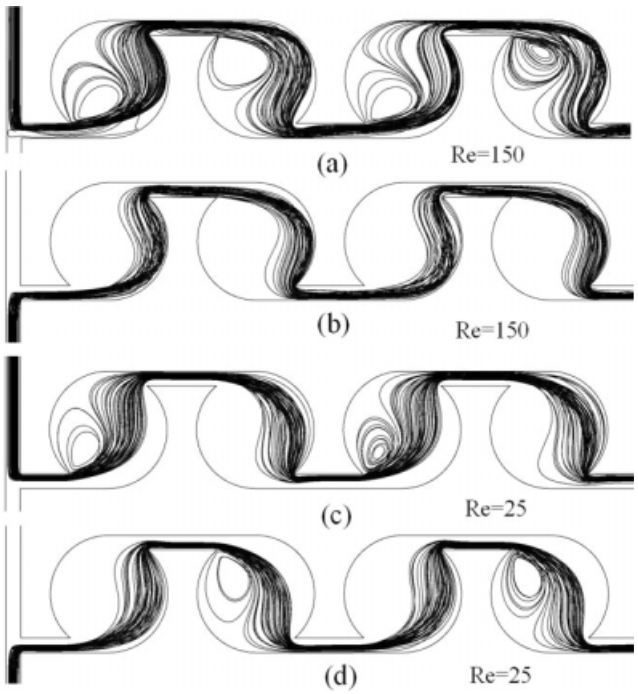

Figure 5. Projected streamlines starting from Inlet 1 and Inlet 2 for $w/d = 1/8$ and $\theta = 0^\circ$.

Figure 5 shows the projected streamlines starting from Inlet 1 and Inlet 2 at $Re = 25$ and $Re = 150$ for $w/d = 1/8$ and $\theta = 0^\circ$. It demonstrates the flow behavior of a single fluid as it passes through circular mixing chambers and constriction channels. The fluid particles that enter a circular chamber experience two different flow patterns: one is a smooth, tangential flow along the channel wall that finally enters the constriction channel; and the other is a circulating flow just downstream of the inlet to the channel, which increases the time of residence of the fluids and thus, the probability of mixing within the chamber. At $Re = 25$, the streamlines of each fluid are along their sidewall and do not cross each other during flow. The recirculation zone in the circular chamber contains only one fluid while the other fluid moves out of the circular channel without being influenced by the zone; hence, mixing is not enhanced very much. Fluid from each inlet forms recirculation zones in alternate circular chambers at $Re = 25$. However, at $Re = 150$, only the fluid from Inlet 1 creates a recirculation zone while the second fluid (from Inlet 2) flows along the wall and does not create a recirculation zone. The streams of both fluids cross each other in the constriction channels at $Re = 150$, which is not the case at $Re = 25$. This is likely to be one of the reasons for the increase in mixing.

Distributions of the mass fraction of the ethanol on the xy-plane at the middle of the channel ($z = 0.05$ mm) in the first two circular mixing chambers and connecting constriction channel are shown in Figure 6 for $w/d = 1/8$ and $\theta = 0^\circ$ at $Re = 25$ and $Re = 50$. It is found that with an increase in the Reynolds number, the increased inertial force tends to shift the interface of the two fluids downstream in the circular chamber. Although the recirculation zone is also present in the circular chamber even at these lower Reynolds numbers as shown in Figure 5, enhancement of mixing is not visible in the recirculation zone. The magnified distribution of the mass fraction in the constriction channel is also shown in each case. It is seen that the mass fraction of the ethanol is almost unchanged in the constriction channel since it is not affected by the turn.

Figure 7 shows the distribution of the mass fraction of ethanol on the xy plane at the middle of the channel at $Re = 150$. The interface of the two unmixed fluids is located very close to the chamber wall near the exit of each chamber, and one of the unmixed streams is confined to a thin layer adjacent to the wall. The streamlines in the constriction channel show the presence of flow recirculation that covers almost

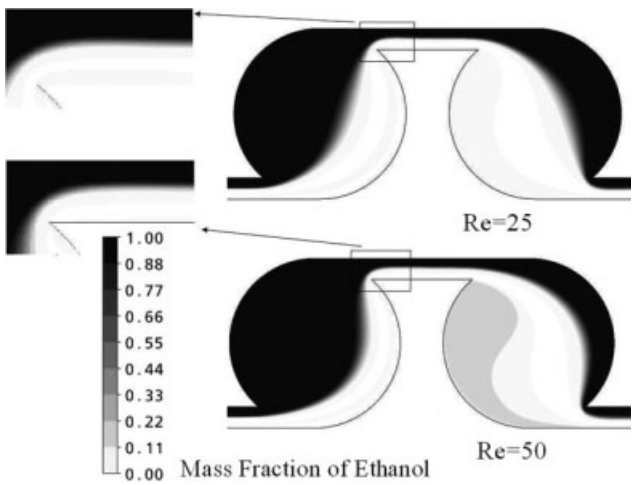

Figure 6. Distributions of the mass fraction of ethanol on the xy-plane at the middle of the channel between the first and second circular mixing chambers for $d/w = 1/8$ and $\theta = 0^\circ$ at $Re = 25$ and 50.

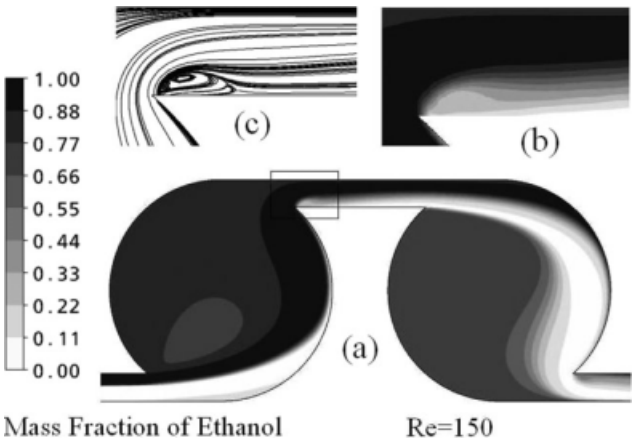

Figure 7. Distributions of the mass fraction of ethanol on the *xy*-plane at the middle of the channel between the first and second circular mixing chambers for *d*/*w* = 1/8 and $\theta = 0^\circ$ at *Re* = 150.

1/3rd of the width of the constriction channel (Figure 7c). This is likely to be a reason for an increase in mixing, as seen from the distribution of the mass fraction in the constriction channel (Figure 7b), which contrasts with the case of lower Reynolds numbers shown in Figure 6. In the recirculation region shown in Figure 5, a substantial enhancement of mixing is achieved at this higher Reynolds number. The zone of unmixed fluid is remarkably reduced in comparison with the case of lower Reynolds numbers shown in Figure 6. The flow recirculation increases the local time of residence and the interface between the fluids in the chamber, and thus promotes mass diffusion. The presence of strong recirculation zones in both the circular mixing chamber and the constriction channel, at the higher Reynolds number (*Re* = 150), has a synergic effect, and hence, accelerates the mixing, as shown in Figure 4.

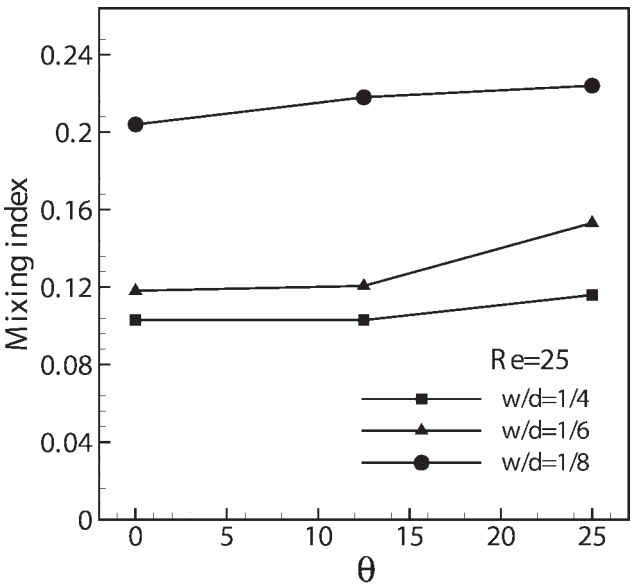

Figure 8. Variation of the mixing index at the end of the device at *Re* = 25.

Effects of geometric parameters

Further calculations for analyzing geometric effects on the mixing and the flow field with the two design variables, i.e., θ and d/w, have been performed at a fixed Reynolds number of 25. This number is above the critical Reynolds number of

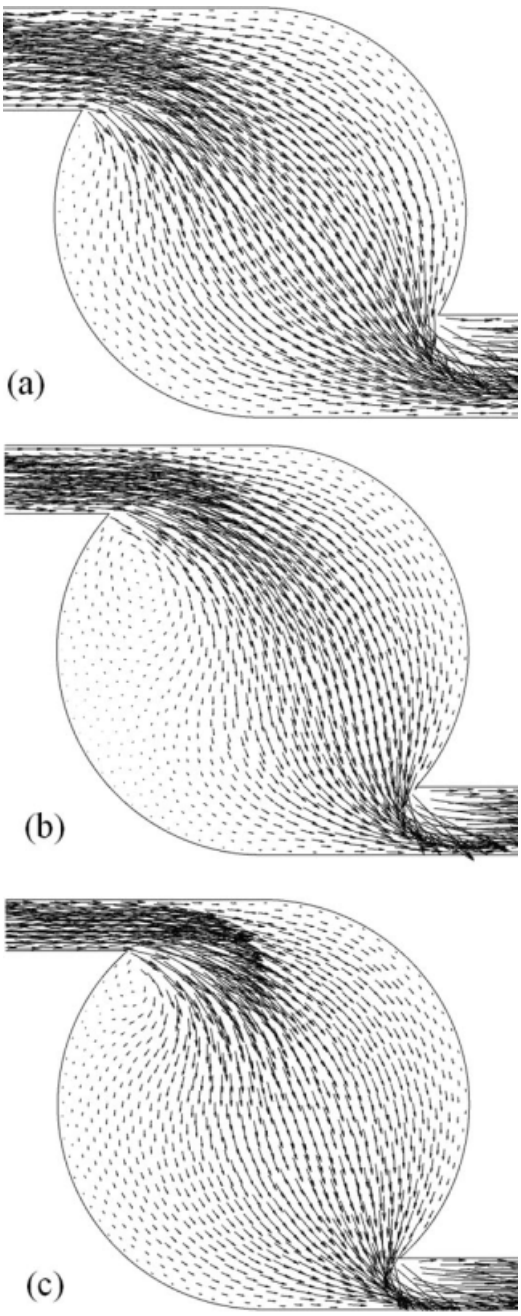

Figure 9. Vector plots on the *xy*-plane at the middle of the channel for $\theta = 0^\circ$ and *Re* = 25.

(a) $w/d = 1/4$; (b) $w/d = 1/6$; and (c) $w/d = 1/8$.

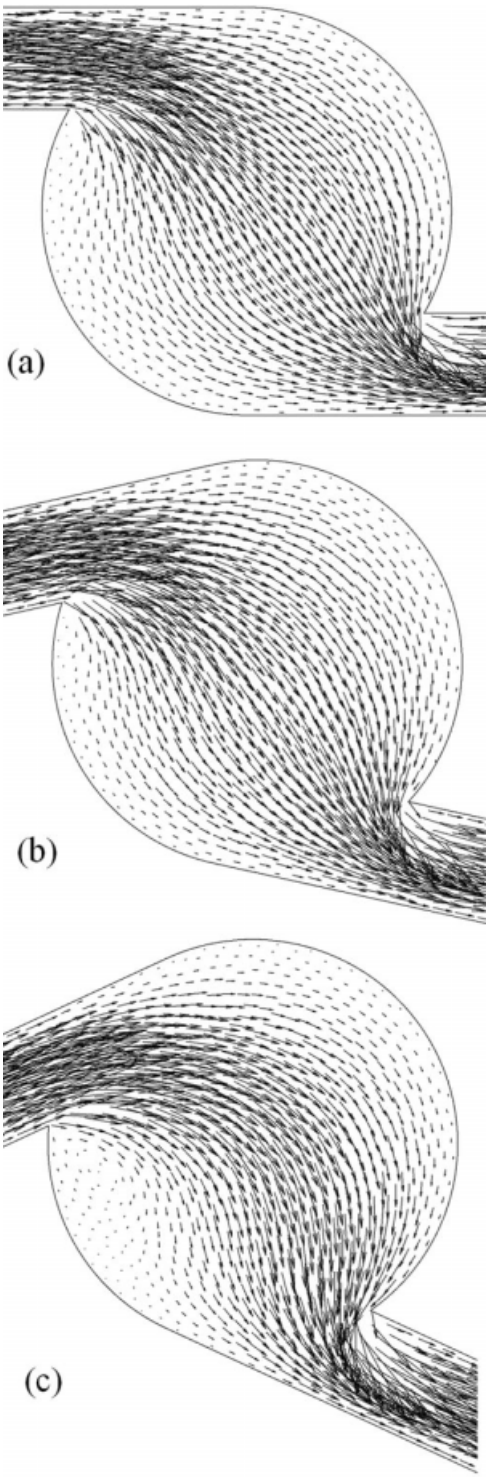

Figure 10. Vector plots on the *xy*-plane at the middle of the channel for *w/d* = 1/4 and *Re* = 25.

(a) $\theta = 0$; (b) $\theta = 12.5$; and (c) $\theta = 25$.

$Re = 20$ (Chung et al.[19]) that is required for developing self-circulation flow in the circular chamber. The analysis has been performed at only a lower Reynolds number because of the large computational time that is entailed at higher Reynolds numbers. Figure 8 shows the effect of θ on the mixing index at the exit of the last circular chamber at $Re = 25$ and for $w/d = 1/4$, 1/6, and 1/8. The results show improvements in the mixing performance of the device with an increase in

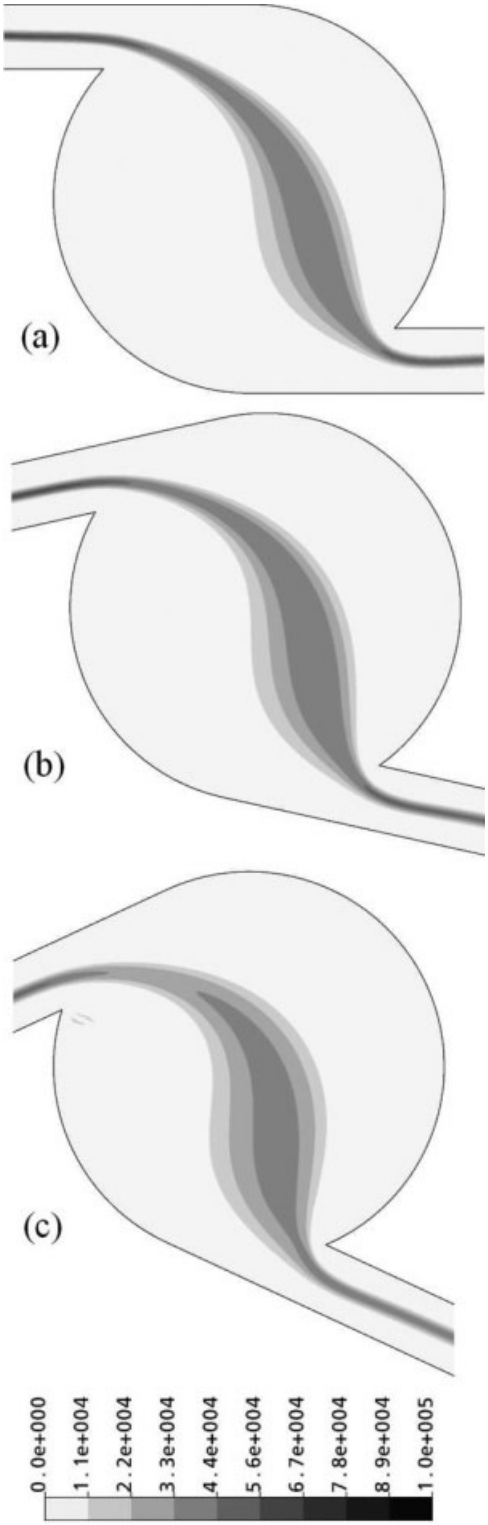

Figure 11. Distributions of the mass fraction gradient of ethanol on the *xy*-plane at the middle of the channel for *w/d* = 1/6 and *Re* = 25.

(a) $\theta = 0$; (b) $\theta = 12.5$; and (c) $\theta = 25$.

θ. A larger value of θ yields a greater change in the direction of flow in the circular chamber before fluid exits the chamber. The mixing performance of the design rapidly increases as the w/d ratio decreases. This is because as w/d decreases, the distance between the two fluid streams reduces in the constriction channel, which results in a shorter distance for diffusion.

Figure 9 shows plots of velocity vectors in the xy-plane at the middle of the channel for $\theta = 0^\circ$ and for $w/d = 1/4$, 1/6, and 1/8 at $Re = 25$. As the value of w/d increases, the velocities of the fluid become greater in the central region of the circular chamber compared to those in the recirculation zone. Further, as the width of the constriction channel decreases, the velocity field becomes more uniform in the circular chamber. Plots of velocity vectors in the xy-plane at the middle of the channel in the second circular mixing chamber are shown in Figure 10 for three different values of θ and for $w/d = 1/4$ and $Re = 25$. The fluids undergo a greater change in the direction of flow in the chamber with increased θ. This is related to the increase in mixing as shown in Figure 8, although the effect is not significant. Figure 11 shows distributions of the mass fraction gradient of ethanol on the xy-plane at the middle of the channel in the second circular mixing chamber for $w/d = 1/6$ and $\theta = 0^\circ$, 12.5°, and 25°. The thickness of the region of high gradient near the center of the chamber increases with θ. This clarifies the increase in mixing with the increase in θ.

Figure 12 shows the variation, with Reynolds number, of the pressure drop in a circular mixing chamber for $\theta = 0^\circ$ and $w/d = 1/8$. The pressure drop rapidly increases with the Reynolds number. Although the circular chamber shows greater efficiency of mixing under a larger Reynolds number, the required pumping power increases significantly as well. The rapid increase in pressure with the Reynolds number is also attributed to the formation of a stronger recirculation zone in both the circular chamber and the constriction channel.

Figure 13 shows the characteristics of the pressure drop as a function of the geometric parameters, w/d and θ. The pressure drop has been calculated for a fixed length of mixers that contain all circular chambers and constriction channels. The trend is very similar to that shown in Figure 8 for the mixing index. The pressure drop increases with increasing θ and decreases with channel width. The results show a stronger dependency of the pressure drop on the width of the constriction channel, as compared with θ. The narrower width of the constriction channel is found to be effective in increasing mixing, but also increases the pressure drop.

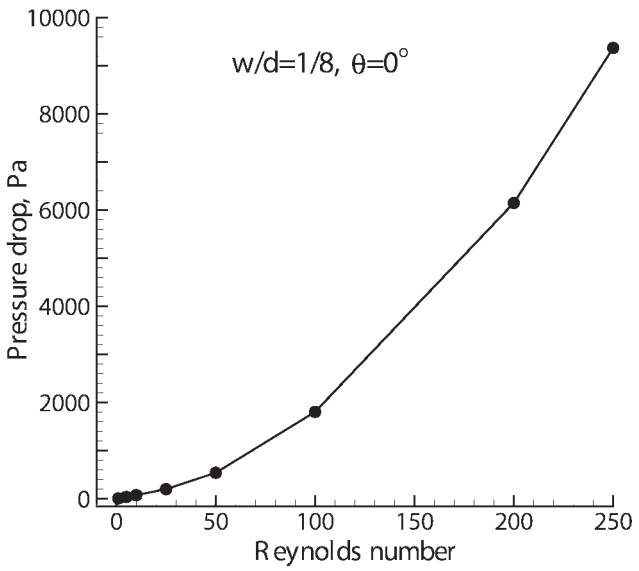

Figure 12. Pressure drop vs. *Re*.

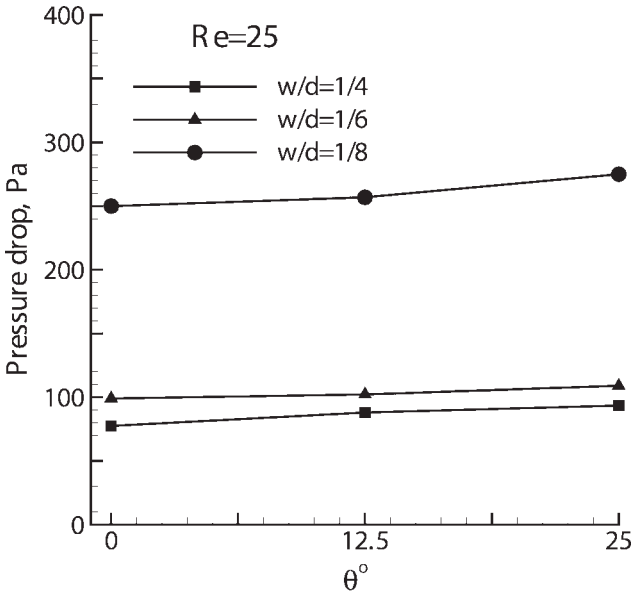

Figure 13. Pressure drop for one circular chamber, as a function of θ.

Conclusions

Numerical simulations have been performed to analyze three-dimensional mixing in a micromixer with four circular mixing chambers. The circular chambers are connected by constriction channels that are intended to induce self-circulating flows in the chambers. The mixing and the flow field have been analyzed for Reynolds numbers ranging from 1 to 250. The device shows minimum mixing performance near a Reynolds number of 5; beyond this value, the performance rapidly improves with the Reynolds number. This rapid increase in mixing performance is influenced by the formation of stronger flow recirculation in both the circular chamber and the constriction channel. However, the pressure drop in the circular chamber significantly increases with the Reynolds number, and hence, the required pumping power increases. The effects of two geometric design variables, namely, the ratio, w/d, of the width of the constriction channel to the diameter of the circular chamber, and the angle, θ, between the outer walls of the chamber and the connection channel, on the mixing and the pressure drop have been investigated at a Reynolds number of 25. The mixing performance improves with an increase in θ and a decrease in w/d, respectively. The influence of w/d on the mixing performance is much stronger than that of θ. The variation of the pressure drop with these two variables is found to be

very similar to the trend for mixing performance. Thus, narrower constriction channels increase the mixing performance as well as the pressure drop.

Acknowledgments

This work was supported by Grant No. R01-2006-000-10039-0 from the Basic Research Program of the Korea Science and Engineering Foundation, and the 2005 Foreign Student Researcher Invitation Program of the Korea Research Foundation.

Notation

c = mass fraction
d = diameter of the circular chamber (m)
D = diffusivity of the fluid ($m^2\ s^{-1}$)
h = channel height (m)
M = mixing index
N = number of sampling points
P_i = pitch of the circular mixing chamber (m)
P = pressure, Pa
Re = Reynolds number
w = channel width (m)

Greek letters

ρ = fluid density ($kg\ m^{-3}$)
μ = absolute viscosity ($kg\ m^{-1}\ s^{-1}$)
σ = variance
θ = angle (degrees)

Literature Cited

1. Nguyen NT, Wu Z. Micromixers—review. *J Micromech Microeng*. 2005;15:R1–R16.
2. Hessel V, Lowe H, Schönfeld F. Micromixers—a review on passive and active mixing principles. *Chem Eng Sci*. 2005;60:2479–2501.
3. Dean WR. Notes on the motion of fluid in curved pipe. *Philos Mag*. 1927;4:208–233.
4. Dean WR. The streamline motion of fluid in curved pipe. *Philos Mag*. 1928;5:673–695.
5. Jiang F, Drese KS, Hardt S, Kupper M, Schönfeld F. Helical flows and chaotic mixing in curved micro channels. *AIChE J*. 2004;50:2297–2305.
6. Schönfeld F, Hardt S. Simulation of helical flows in microchannels. *AIChE J*. 2004;50:771–778.
7. Sudarsan AP, Ugaz VM. Fluid mixing in planar spiral microchannels. *Lab Chip*. 2006;6:74–82.
8. Sudarsan AP, Ugaz VM. Multivortex micromixing. *Proc Natl Acad Sci USA*. 2006;103:7228–7233.
9. Vanka SP, Luo G, Winkler CM. Numerical study of scalar mixing in curved channels at low Reynolds numbers. *AIChE J*. 2004;50:2359–2368.
10. Kumar V, Aggarwal M, Nigam KDP. Mixing in curved tubes. *Chem Eng Sci*. 2006;61:5742–5753.
11. Yamaguchi Y, Takagi F, Yamashita K, Nakamura H, Maeda H. 3-D. Simulation and visualization of laminar flow in a microchannel with hair-pin curves. *AIChE J*. 2004;50:1530–1535.
12. Hong CC, Choi J-W, Ahn CH. A novel in-plane passive microfluidic mixer with modified Tesla structures. *Lab Chip*. 2004;4:109–113.
13. Lee SW, Lee SS. Rotation effect in split and recombination micromixing. *Sens Actuators B*. 2008;129:364–371.
14. Chang S, Cho Y-H. Static micromixers using alternating whirls and lamination. *J. Micromech Microeng*. 2005;15:1397–1405.
15. Park SJ, Kim JK, Park J, Chung S, Chung C, Chang JK. Rapid three-dimensional passive rotation micromixer using the breakup process. *J Micromech Microeng*. 2004;14:6–14.
16. Jeon MK, Kim JH, Noh J, Kim SH, Park HG, Woo SI. Design and characterization of a passive recycle micromixer. *J Micromech Microeng*. 2005;15:346–350.
17. Lin CH, Tsai CH, Fu LM. A rapid three-dimensional vortex micromixer utilizing self-rotation effects under low Reynolds number conditions. *J Micromech Microeng*. 2005;15:935–943.
18. Lin CH, Tsai CH, Pan CW, Fu LM. Rapid circular microfluidc mixer utilizing unbalanced driving force. *Biomed Microdevices*. 2007;9:43–50.
19. Chung YC, Hsu YL, Jen CP, Lu MC, Lin YC. Design of passive mixers utilizing microfluidic self-circulation in the mixing chamber. *Lab Chip*. 2004;4:70–77.
20. Jin S-Y, Liu Y-Z, Wang W-Z, Cao ZM. Numerical evaluation of two-fluid mixing in a swirl micro-mixer. *J Hydrodynamics Ser B*. 2006;18:5:542–546.
21. Hu Y-H, Chang M. Study in the design of micromixer and inspection of mixing efficiency. *Proc SPIE*. 2003;526:1–8.
22. CFX-11.0,Solver Theory, ANSYS, 2006.
23. Leonard BP. Locally modified QUICK scheme for highly convective 2D and 3D flows. In: Proceedings of the International Conference on Numerical Methods in Laminar and Turbulent Flow, Part 1, Pineridge Press, Swansea, 1987.
24. Noll B. *Numerische Stromungsmechank*. Springer: Berlin, 1993.
25. Hardt S, Schönfeld F. Laminar mixing in different interdigital micromixers. II. Numerical simulations. *AIChE J*. 2003;49:578–584.

Manuscript received Aug. 8, 2008, and revision received Dec. 13, 2008.